

# Blast Mitigation in a Sandwich Composite Using Graded Core and Polyurea Interlayer

N. Gardner · E. Wang · P. Kumar · A. Shukla

Received: 23 December 2010 / Accepted: 23 May 2011  
© Society for Experimental Mechanics 2011

**Abstract** The dynamic behavior of two types of sandwich composites made of E-Glass Vinyl-Ester (EVE) facesheets and Corecell™ A-series foam with a polyurea interlayer was studied using a shock tube apparatus. The materials, as well as the core layer arrangements, were identical, with the only difference arising in the location of the polyurea interlayer. The foam core itself was layered with monotonically increasing wave impedance of the core layers, with the lowest wave impedance facing the shock loading. For configuration 1, the polyurea interlayer was placed behind the front facesheet, in front of the foam core, while in configuration 2 it was placed behind the foam core, in front of the back facesheet. A high-speed side-view camera, along with a high-speed back-view 3-D Digital Image Correlation (DIC) system, was utilized to capture the real time deformation process as well as mechanisms of failure. Post mortem analysis was also carried out to evaluate the overall blast performance of these two configurations. The results indicated that applying polyurea behind the foam core and in front of the back facesheet will reduce the back face deflection, particle velocity, and in-plane strain, thus improving the overall blast performance and maintaining structural integrity.

**Keywords** Sandwich structures · Functionally graded material · Polyurea interlayer · Blast loading · High speed photography

---

N. Gardner · E. Wang (SEM member) ·  
P. Kumar (SEM member) · A. Shukla (✉, SEM fellow)  
Dynamic Photomechanics Laboratory, Department of Mechanical,  
Industrial & Systems Engineering, University of Rhode Island,  
92 Upper College Road,  
Kingston, RI 02881, USA  
e-mail: shuklaa@egr.uri.edu

## Introduction

Core materials play a crucial role in the dynamic behavior of sandwich structures when they are subjected to high-intensity impulse loadings such as air blasts. Their properties assist in dispersing the mechanical impulse that is transmitted into the structure and thus protect anything located behind it [1–3]. Stepwise graded materials, where the material properties vary gradually or layer by layer within the material itself, were utilized as a core material in sandwich composites due to the fact that their properties can be designed and controlled. Typical core materials utilized in blast loading applications are generally foam, due to their ability to compress and withstand highly transient loadings. In recent years, with its ability to improve structural performance and damage resistance of structures, as well as effectively dissipate blast energy, the application of polyurea to sandwich structures has become a new area of interest

The numerical investigation by Apetre et al. [4] on the impact damage of sandwich structures with a graded core (density) has shown that a reasonable core design can effectively reduce the shear forces and strains within the structures. Consequently, they can mitigate or completely prevent impact damage on sandwich composites. Li et al. [5] examined the impact response of layered and graded metal-ceramic structures numerically. They found that the choice of gradation has a great significance on the impact applications and the particular design can exhibit better energy dissipation properties. In their previous work, the authors experimentally investigated the blast resistance of sandwich composites with stepwise graded foam cores [6]. Two types of core configurations were studied and the sandwich composites were layered / graded based on the

densities of the given foams, i.e. monotonically and non-monotonically. The results indicated that monotonically increasing the wave impedance of the foam core, thus reducing the wave impedance mismatch between successive foam layers, will introduce a stepwise core compression, greatly enhancing the overall blast resistance of sandwich composites.

Although the behavior of polyurea has been investigated [7–10], there have been no studies regarding the dynamic behavior of functionally graded core with a polyurea interlayer. Tekalur et al. [11] experimentally studied the blast resistance and response of polyurea based layered composite materials subjected to blast loading. Results indicated that sandwich materials prepared by sandwiching the polyurea between two composite skins had the best blast resistance compared to the EVE composite and polyurea layered plates. Bahei-El-Din et al. [12] numerically investigated the blast resistance of sandwich plates with a polyurea interlayer under blast loading. Their results suggest that separating the composite facesheet from the foam core by a thin interlayer of polyurea can be very beneficial in comparison to the conventional sandwich plate design. Amini et al. [13–16] experimentally and numerically studied the dynamic response of circular monolithic steel and steel-polyurea bilayer plates to impulsive loads. More importantly they focused on the significance of the relative position of the polyurea layer with respect to the loading direction. Results indicated that the polyurea layer can have a significant effect on the response of the steel plate to dynamic impulsive loads, both in terms of failure mitigation and energy absorption, if it is placed on the back face of the plate. On the contrary, they also found that polyurea can enhance the destructive effect of the blast, promoting (rather than mitigating) the failure of the steel plate if applied on the impact side of the plate.

The present study focuses on the blast response of sandwich composites with a functionally graded core and a polyurea (PU) interlayer. Two different core layer configurations were investigated, with the only difference arising in the location of the polyurea (PU) interlayer. The quasi-static and dynamic constitutive behaviors of the foam core materials, as well as the polyurea, were first experimentally studied using a modified SHPB device with a hollow transmitted bar. The sandwich composites were then subjected to shock wave loading generated by a shock tube. The shock pressure profiles, real time deflection images, and post mortem images were carefully analyzed to reveal the mechanisms of dynamic failure of these sandwich composites. Digital Image Correlation (DIC) analysis was implemented to investigate the real time deflection, strain, and particle velocity.

## Material and Specimen

### Skin and Core Materials

The skin materials that were utilized in this study are E-Glass Vinyl-Ester (EVE) composites. The woven roving E-glass fibers of the skin material were placed in a quasi-isotropic layout [0/45/90/−45]<sub>s</sub>. The fibers were made of the 0.61 kg/m<sup>2</sup> areal density plain weave. The resin system used was Ashland Derakane Momentum 8084, with the front and back skins (facesheets) consisting of identical layups and materials. Figure 1 shows a schematic of the sandwich composite with skin and core materials.

The foam core materials used in the present study are Corecell™ A-series styrene acrylonitrile (SAN) foams, which are manufactured by Gurit SP Technologies specifically for marine sandwich composite applications. The three types of Corecell™ A series foam that were used in present study were A300, A500, and A800. The polyurea used in the present study is Dragonshield-HT, which is manufactured by Specialty Products Incorporated (SPI) specifically for blast resistance and mitigation. It is a state-of-the-art high performance, sprayed, plural component pure elastomer, based on amine-terminated polyether resins, amine chain extenders and MDI prepolymers. Table 1 lists important material properties from the manufacturer's data of the three foams [17], as well as the Dragonshield-HT polyurea [18] and the material properties of the facesheet as determined using ASTM standards. In Table 1, the A300 foam has the lowest nominal density ( $\rho$ ), as well as compressive modulus ( $E$ ) of the three foams, followed by the A500 and A800 foams respectively. Since both the nominal density and the compressive modulus are increasing from A300 to A800 foam, the wave impedance also increases.

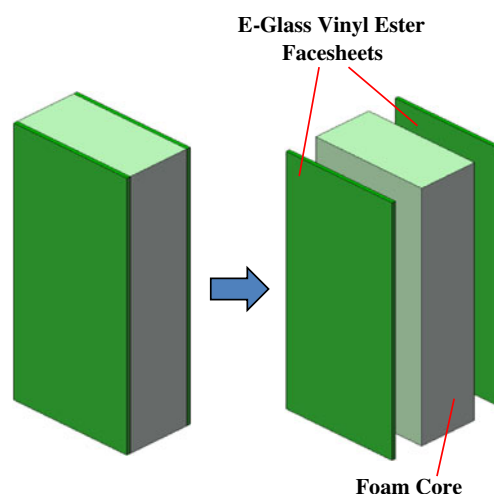


Fig. 1 Schematic of sandwich composite with skin and core

**Table 1** Material properties for foam core [17] and polyurea [18]

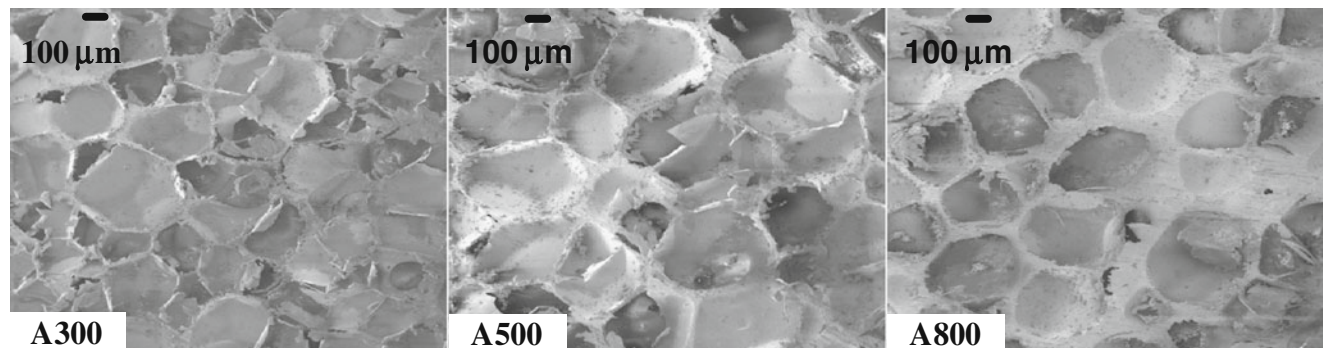
	Nominal density, $\rho$ (kg/m <sup>3</sup> )	Compressive modulus, E (MPa)	Compressive strength, $\sigma_y$ (MPa)	Elongation ( % )
A300	58.5	32	.5	–
A500	92	64	.9	–
A800	150	117	2.1	–
Dragonshield-HT	1000	8.9	–	619
E-Glass Vinyl-Ester Composite	1800	13,600	220	–

The cell structures for the three foams are very similar and the only difference appears in the cell wall thickness and node sizes, which accounts for the different densities of the foams. The SEM images of the cell microstructures can be seen in Fig. 2

#### Sandwich Panels with Stepwise Graded Core Layer Arrangement and PU Interlayer

The VARTM process was utilized to fabricate the sandwich specimens. The overall dimensions for the samples were 102 mm wide, 254 mm long and 48 mm thick. The total thickness of the core was 38 mm, with a skin thickness of 5 mm. The core consisted of three layers of foam (A300/A500/A800—low/middle/high density) and a polyurea (PU) interlayer. The first two layers of the foam core (A300 / A500) were each 12.7 mm thick, while the third foam layer (A800) was 6.35 mm. The polyurea interlayer was 6.35 mm. The average areal density of the samples was 26 kg/m<sup>2</sup>.

Two core configurations, which consisted of identical core materials, were studied (as shown in Fig. 3(a)). For configuration 1, the polyurea interlayer was placed behind the front facesheet and in front of the foam core (PU/A300/A500/A800). For configuration 2, the polyurea interlayer was placed behind the foam core, and in front of the back facesheet (A300/A500/A800/PU). With these configurations it should be noted that the first core layer is the one first subjected to the shock wave loading. Actual samples can be seen in Fig. 3(b).

**Fig. 2** Cell microstructure of foam core layers

#### Experimental Setup and Procedure

##### Modified Split Hopkinson Pressure Bar with Hollow Transmission Bar

Split Hopkinson Pressure Bar (SHPB) is the most common device for measuring dynamic constitutive properties of materials. Due to the low-impedance of Corecell™ foam materials, dynamic experiments for the core materials were performed with a modified SHPB device with a hollow transmission bar to increase the intensity of the transmitted signal. A sketch of the modified SHPB device and typical pulse profiles are given in Fig. 4. It has a 304.8 mm-long striker, 1600 mm-long incident bar and 1447 mm-long transmission bar. All of the bars are made of a 6061 aluminum alloy. The nominal outer diameters of the solid incident bar and hollow transmission bar are 19.05 mm. The hollow transmission bar has a 16.51 mm inner diameter. At the head and at the end of the hollow transmission bar, end caps made of the same material as the bar were press fitted into the hollow tube. By applying pulse shapers, the effect of the end caps on the stress waves can be minimized. The details of the analysis and derivation of equations for analysis of experimental data can be found in ref [19].

##### Shock Tube

The shock tube apparatus was utilized to obtain the controlled blast loading (Fig. 5(a)). It has an overall length of 8 m, consisting of a driver, driven and muzzle section.

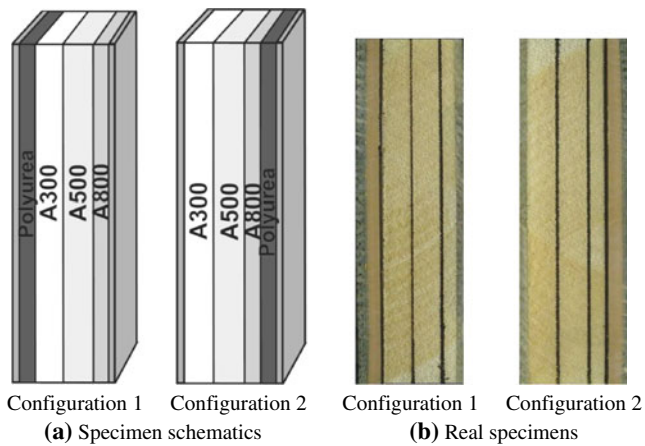


**Fig. 3** Specimen configuration and core gradation

The high-pressure driver section and the low pressure driven section are separated by a diaphragm. By pressurizing the high-pressure section, a pressure difference across the diaphragm is created. When this difference reaches a critical value, the diaphragm ruptures. This rapid release of gas creates a pressure wave that develops into a shock wave as it travels down the tube to impart dynamic loading on the specimen.

Figure 5(b) shows detailed dimensions and locations of the muzzle, specimen, supports and the pressure sensors (PCB102A). The sensors are mounted at the end of the muzzle section to measure the incident pressure and the reflected pressure during the experiment. The final muzzle diameter is 0.0762 m. The distance between the two sensors is 0.16 m and the distance between the second sensor and the end of the muzzle is  $\sim 0.02$  m. The specimen was placed in the supports and positioned close to the end of the muzzle. These support fixtures ensure simply supported boundary conditions with a 0.1524 m span.

#### High Speed Photography Systems

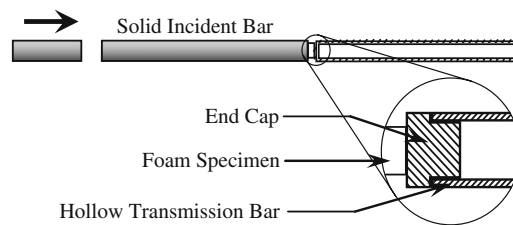
Two high-speed photography systems were used in the present study, as shown in Fig. 6. A high-speed 3-D Digital Image Correlation (DIC) system, consisting of two high-

speed digital cameras [Photron SA1], was placed on the back side of the specimen to obtain the real-time full-field in-plane strain, along with out-of-plane deflection and velocity of the back facesheet. A speckle pattern was placed directly on the back facesheet of the sandwich composite to ensure good contrast of the images. Another high-speed digital camera, [Photron SA1], was placed perpendicular to the side surface of the specimen to capture the side-view deformation images. A framing rate of 20,000 fps was utilized which gives an interframe time of approximately 50  $\mu$ s.

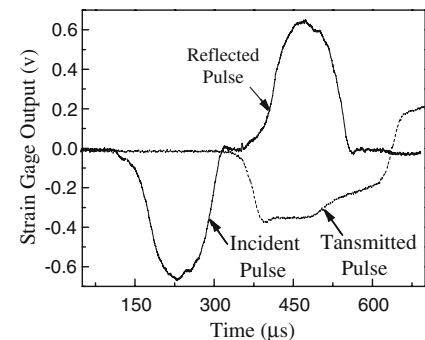
#### Experimental Procedure and Parameters

An initial series of experiments was conducted for both configurations and three samples were tested for each. This was followed by a second set of experiments, in which two specimens were tested for each configuration. Two different loading conditions were applied. For the first set of experiments, a simply stacked diaphragm of 5 plies of 10 mil mylar sheets with a total thickness of 1.27 mm was utilized to generate an impulse loading on the specimen with an incident peak pressure of approximately 1.0 MPa, a reflected peak pressure of approximately 5.0 MPa and a wave speed of approximately 1000 m/s. A typical pressure profile obtained from the transducer closest to the specimen ( $\sim 0.02$  m away) can be seen in Fig. 7. It should be noted that both pressure transducers were utilized to obtain the shock wave history, i.e. incident / reflected pressure and incident / reflected velocity. However, only the pressure transducer closest to the specimen was used to obtain the pressure applied on the specimen. For the second set of experiments, a simply stacked diaphragm of 10 plies of 10 mil mylar sheets with a total thickness of 2.54 mm was utilized to generate an impulse loading on the specimen with an incident peak pressure of approximately 1.5 MPa, a reflected peak pressure of approximately 7.5 MPa, and a wave speed of approximately 1300 m/s. Due to the authors previous work [6], the experiments corresponding to the loading conditions with an incident peak pressure of  $\sim 1.0$  MPa will be presented and discussed in detail, while

**Fig. 4** Sketch of modified SHPB device with hollow transmission bar and typical pulse profiles

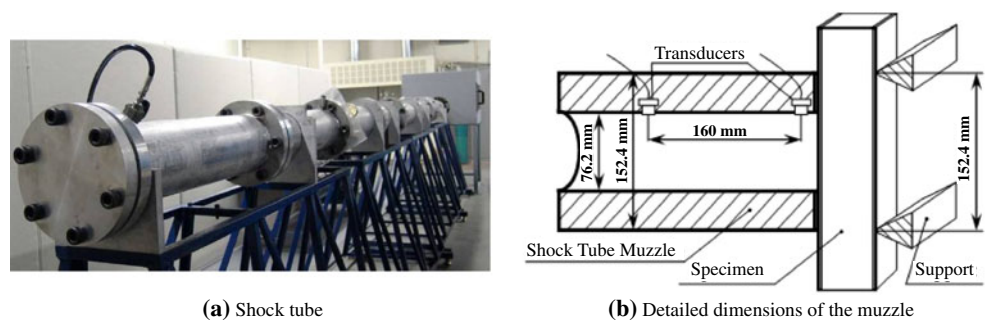


**(a)** Modified SHPB device



**(b)** Typical pulse profiles

Fig. 5 Shock tube apparatus



the experiments corresponding to the higher loading conditions (incident peak pressure  $\sim 1.5$  MPa) will be utilized to better evaluate the performance and failure mechanisms of the sandwich structures.

## Experimental Results and Discussion

### Dynamic Behavior of Core Material

The quasi-static and dynamic true stress-strain curves for the core materials under compressive loading are obtained and shown in Fig. 8. The four types of core materials used in the present study have different quasi-static and dynamic behavior. For the same type of Corecell™ A foam and Dragonshield-HT polyurea, the material behavior under high strain rate loading is significantly different from its behavior under quasi-static loading.

The yield stresses of core materials under quasi-static and high strain rate loading are listed in Table 2. The dynamic yield stress of A500 and A800 increases approximately 100% in comparison to their quasi-static yield stress, while the dynamic yield stress of A300 increases approximately 50% in comparison to its quasi-static yield stress. Also it can

be observed that the high strain-rate yield stress of Dragonshield-HT polyurea increases approximately 200% in comparison to its quasi-static yield stress. The improvement of the mechanical behavior from quasi-static to high strain-rates for all core materials used in the present study signifies their ability to absorb more energy under high strain-rate dynamic loading.

### Response of Sandwich Composites with Graded Cores

#### Real-time deformation

The real-time observations of the transient behavior for both core configurations subjected to shock wave loading are shown in Figs. 9 and 10. The shock wave propagates from the right side of the image to the left side and some detailed deformation and failure mechanisms are pointed out in the figures. The time frames used to represent the blast loading event are chosen in a manner so they can be correlated to the time in which these damage mechanisms were first observed.

The real-time blast loading response of configuration 1 (PU/A300/A500/A800) is shown in Fig. 9. It can be observed from the images that indentation failure (initiation of core compression) begins at approximately  $t=150 \mu\text{s}$ . Following indentation failure, core delamination is first observed at  $t=400 \mu\text{s}$ , and occurs at the bottom of the specimen between the polyurea interlayer and the first layer of foam core. By  $t=550 \mu\text{s}$  more core delamination is observed at the top of the specimen, again between the polyurea interlayer and the first layer of foam core. Also at this time two central core cracks have initiated where the supports are located, and heavy core compression is present in the first layer of the foam core (A300). By  $t=1150 \mu\text{s}$ , the first layer of foam core (A300) has reached a maximum level of compression (8 mm), approximately 75% of its original thickness (12.7 mm). After this time, the response is global bending of the specimen and by  $t=1800 \mu\text{s}$ , no new failure mechanisms were observed. Also the core cracks have propagated through the foam core to the polyurea interlayer and there is heavy core delamination between the polyurea interlayer and the foam core.

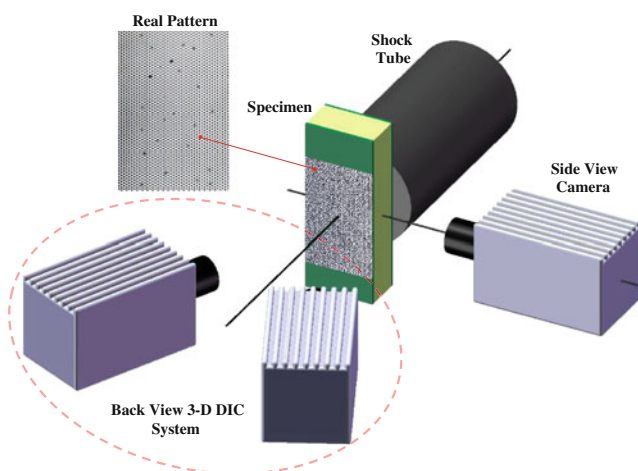


Fig. 6 High-speed photography set-up (back-view DIC and side-view)

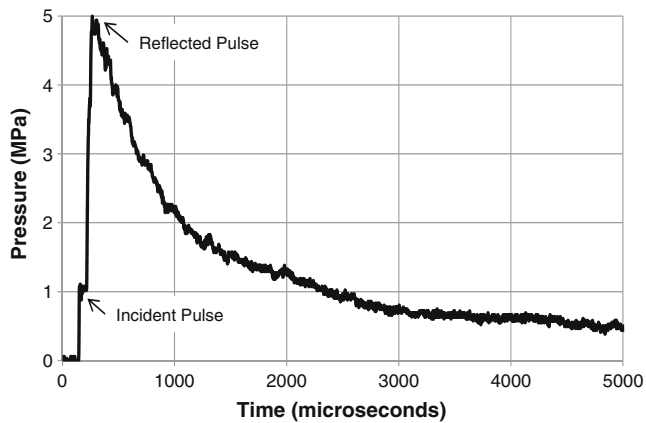


Fig. 7 Incident and reflected pressure profiles

The real-time blast loading response of configuration 2 (A300/A500/A800/PU) is shown in Fig. 10. It is evident from the figure that indentation failure begins at  $t=150 \mu\text{s}$ . After indentation failure is observed, heavy core compression is observed in the first core layer (A300 foam). By  $t=650 \mu\text{s}$  the first layer of foam (A300) has compressed to a maximum, reaching its densification level, and the shock wave has now propagated into the second foam core layer (A500), initiating compression of this core layer. Also at this time, a core crack has initiated at the bottom of the specimen where the support is located. Skin delamination is evident between the front skin and the foam core, and is located at the bottom of the specimen. At  $t=1150 \mu\text{s}$  skin delamination can be observed at the top of the specimen between the front facesheet and the foam core. Also at this time, the compression in the second foam core layer has increased to its maximum and no more compression is observed in the core, resulting in a global bending response. Between  $t=1150 \mu\text{s}$  and  $t=1800 \mu\text{s}$ , no new failure mechanisms were observed. The core crack continues to propagate through the third layer of the foam core (A800)

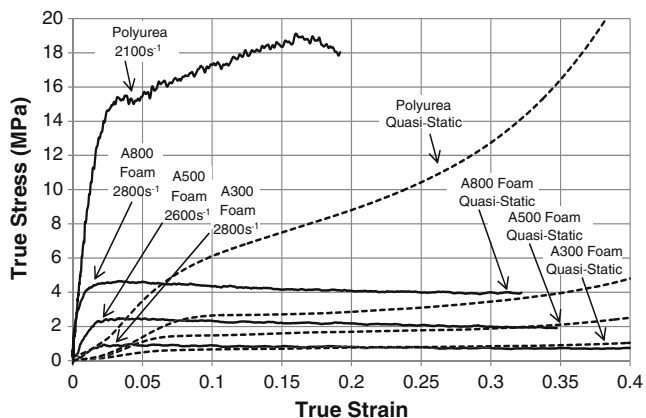


Fig. 8 Quasi-static and high strain-rate compressive behaviors of the different types of core materials

Table 2 Yield strength of core materials

Foam Type	A300	A500	A800	Polyurea
Quasi-Static (MPa)	0.60	1.35	2.46	5.38
High Strain-Rate (MPa)	0.91	2.47	4.62	15.48

and skin delamination at the bottom of the specimen has increased between the front facesheet and the foam core.

Comparing the deformation mechanisms observed in configuration 1 and configuration 2, the location of the polyurea interlayer affects the order and level of different failure mechanisms, such as core compression, core cracking and interface delamination, as well as the time at which they are first observed. In configuration 1, indentation failure (core compression) is followed by delamination in the core and then core cracking. Unlike configuration 1, the indentation failure of configuration 2 is followed by heavy core compression, core cracking and then skin delamination. Comparing both configurations, the indentation failure is observed at approximately the same time, while core cracking and delamination initiate earlier in configuration 1 than in configuration 2, approximately  $100 \mu\text{s}$  and  $250 \mu\text{s}$  respectively.

The location of the polyurea interlayer also affects the core deformation mode for each configuration. In configuration 1 the initial blast loading is uniformly distributed over the polyurea layer, resulting in a global uniform compression of the first layer of the foam core (A300). On the contrary, in configuration 2 the initial impulse is non-uniformly distributed into the foam core, resulting in a local compression in the central region of the first layer of the foam core (A300) where the shock loading was applied. This indicates that the polyurea interlayer has the ability to disperse the shock loading.

Also the deformation shape for both configurations is much different. For configuration 1, the specimen exhibits a double-winged deformation shape until approximately  $t=400\text{--}500 \mu\text{s}$ , then the polyurea layer begins to delaminate from the core, exhibiting a shape much like a specimen in pure bending. For configuration 2, the specimen exhibits a double-winged deformation shape throughout the entire blast loading event. Therefore, configuration 2 has the ability to support the shear stresses that are present during the event, while configuration 1 could not.

### Deflection

The mid-point deflections of the constituents of the sandwich composites with different core configuration were obtained from the high speed side-view images and shown in Fig. 11. For configuration 1, the mid-point deflection of the front face (front skin), interface 1 (between first and

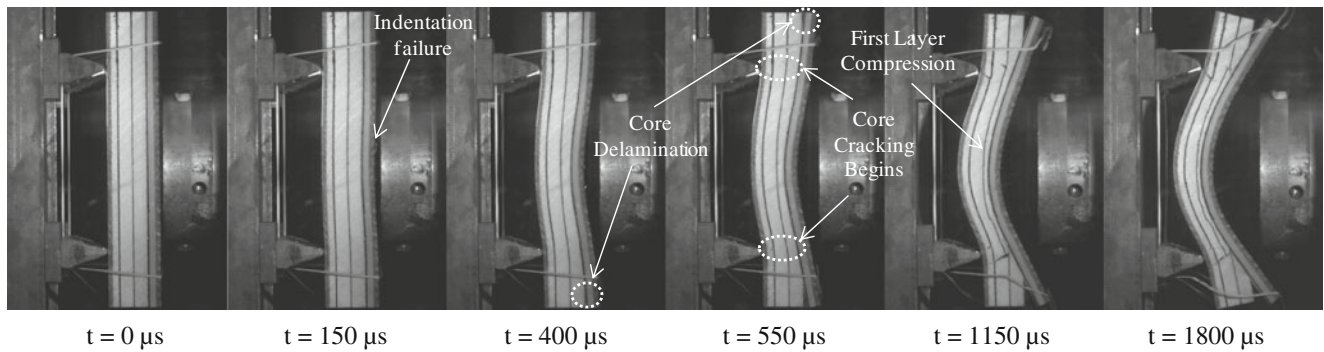


**Fig. 9** High speed images for configuration 1 (PU/A300/A500/A800)

second core layer), interface 2 (between second and third core layer), interface 3 (between third and fourth core layer), and back face (back skin) were plotted and are shown in Fig. 11(a). The front face and interface 1 deflect in the same manner to the same value of approximately 43 mm at  $t = 1800 \mu\text{s}$ , while interface 2, interface 3, and the back face deflect in a similar manner to approximately 34 mm. Since the front face and interface 1 deflect in the same manner to the same value (43 mm), it signifies that the polyurea interlayer, which is located between the front face and interface 1, exhibits no compression. The difference between the deflection of interface 1 and interface 2 indicates the total amount of compression observed in the second core layer, which is the first layer of foam (A300). It can be seen that the A300 layer of foam compressed approximately 9 mm, which is 75% of its original thickness (12.7 mm). Since interface 2, interface 3, and the back face all deflected in a similar manner to the same value of approximately 34 mm, it can be concluded that the A500 foam layer (located between interface 2 and interface 3) and the A800 foam layer (located between interface 3 and the back face) showed no compression. Therefore the core layer arrangement of configuration 1 allows for compression only in the A300 layer of foam and has a front face and back face deflection of approximately 43 mm and 34 mm respectively.

For configuration 2, the mid-point deflection of the front face (front skin), interface 1 (between first and second core layer), interface 2 (between second and third core layer), interface 3 (between third and fourth core layer), and back face (back skin) were plotted and are shown in Fig. 11(b). The front face deflected to approximately 33 mm  $t = 1800 \mu\text{s}$ , while interface 1 deflected to approximately 24 mm, and interface 2, interface 3 and the back face deflected in the same manner to a value of 21 mm respectively. The difference between the front face deflection and the deflection of interface 1 signifies the amount of compression in the first core layer (A300 foam). Therefore it can be observed that the A300 foam layer compressed approximately 9 mm, or 75% of its original thickness (12.7 mm). Again, noting the difference between the deflection of interface 1 and interface 2 the amount of compression in the second core layer (A500 foam) can be obtained. By inspection the A500 foam core layer compresses approximately 3 mm, which is approximately 25% of its original thickness. Finally, since interface 2, interface 3 and the back face all deflected in a similar manner to approximately the same value of 21 mm, it can be concluded that there was no compression in the third and fourth core layer (A500 foam layer and the polyurea interlayer). Therefore, the core arrangement of configuration 2 allows for a stepwise compression through the core

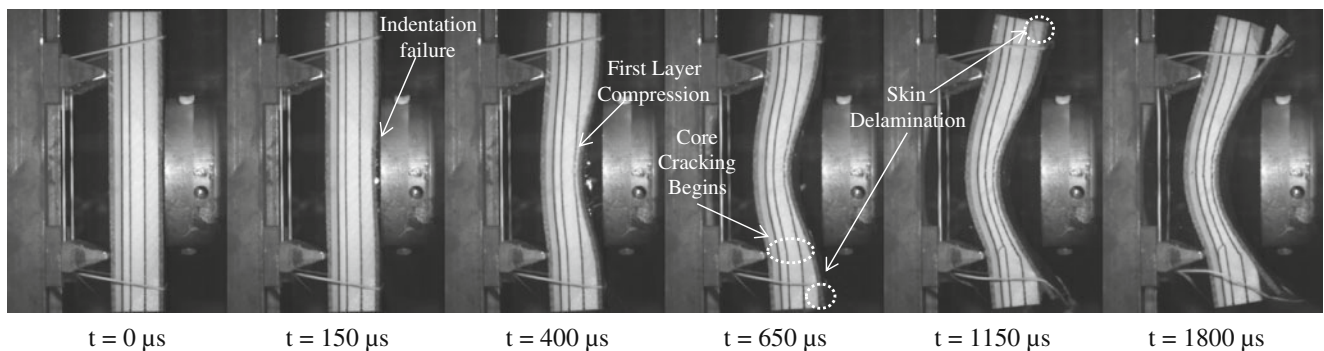


**Fig. 10** High speed images for configuration 2 (A300/A500/A800/PU)

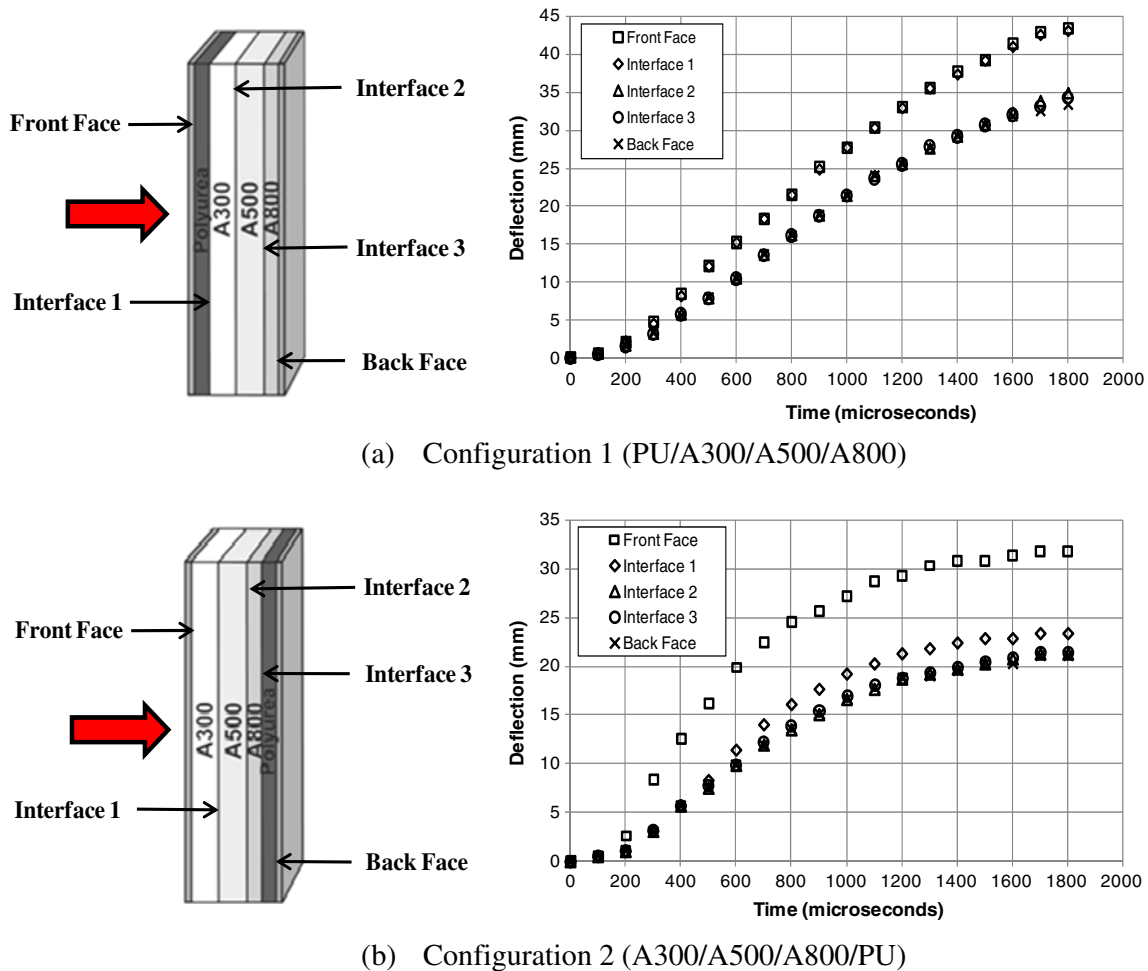


Fig. 11 Mid-point deflection of both configurations

and the front face and back face deflect to approximately 33 mm and 21 mm respectively.

From the deflection data of each interface in Fig. 11, the deformation of each core layer along the mid-line (line of symmetry) can be obtained by subtracting the core layers' back side deflection from the core layers' front side deflection. Sequentially, the strain and strain rate along the line of symmetry of each core layer can be obtained using the following equations,

$$\text{strain} = \varepsilon = \frac{(\Delta l)}{l_{\text{original}}} \quad (1)$$

$$\text{strain rate} = \frac{d\varepsilon}{dt} = \frac{d}{dt} \left( \frac{(\Delta l)}{l_{\text{original}}} \right) = \frac{1}{l_{\text{original}}} \left( \frac{d(\Delta l)}{dt} \right) \quad (2)$$

where,  $l_{\text{original}}$  is the original thickness of the each core layer and  $\Delta l/dt$  is the deformation rate.

The strain and strain rate histories of the core layers for each configuration, as calculated from equations (1) and (2) using the mid-point deflection data from Fig. 11 are shown

in Fig. 12. For those layers exhibiting no compression, their strain and strain rate results ( $0 \text{ s}^{-1}$ ) are not shown here. The strain results are shown in Fig. 12(a) and (b), while the strain rate results are shown in Fig. 12(c) and (d).

It can be seen that in both configurations, the A300 foam layer exhibits approximately the same amount of maximum strain, however the time in which the maximum strain was reached varied. For configuration 1, distributing the initial loading uniformly results in densification of the A300 foam much later in the deformation history, more mitigation of the initial shock loading and thus less transmission of the load to the A500 layer, resulting in no compression in this layer. For configuration 2, unlike configuration 1, localized loading allowed for densification of the A300 foam layer much earlier in the deformation history, and consequently transmitted more shock loading into the A500 layer. Therefore, the A500 layer also showed compression. However, the deformation in configuration 2 is constrained to the central region where the initial loading was applied.

The strain rate plots of configuration 1 and configuration 2 show that the A300 layer of configuration 2 reached a

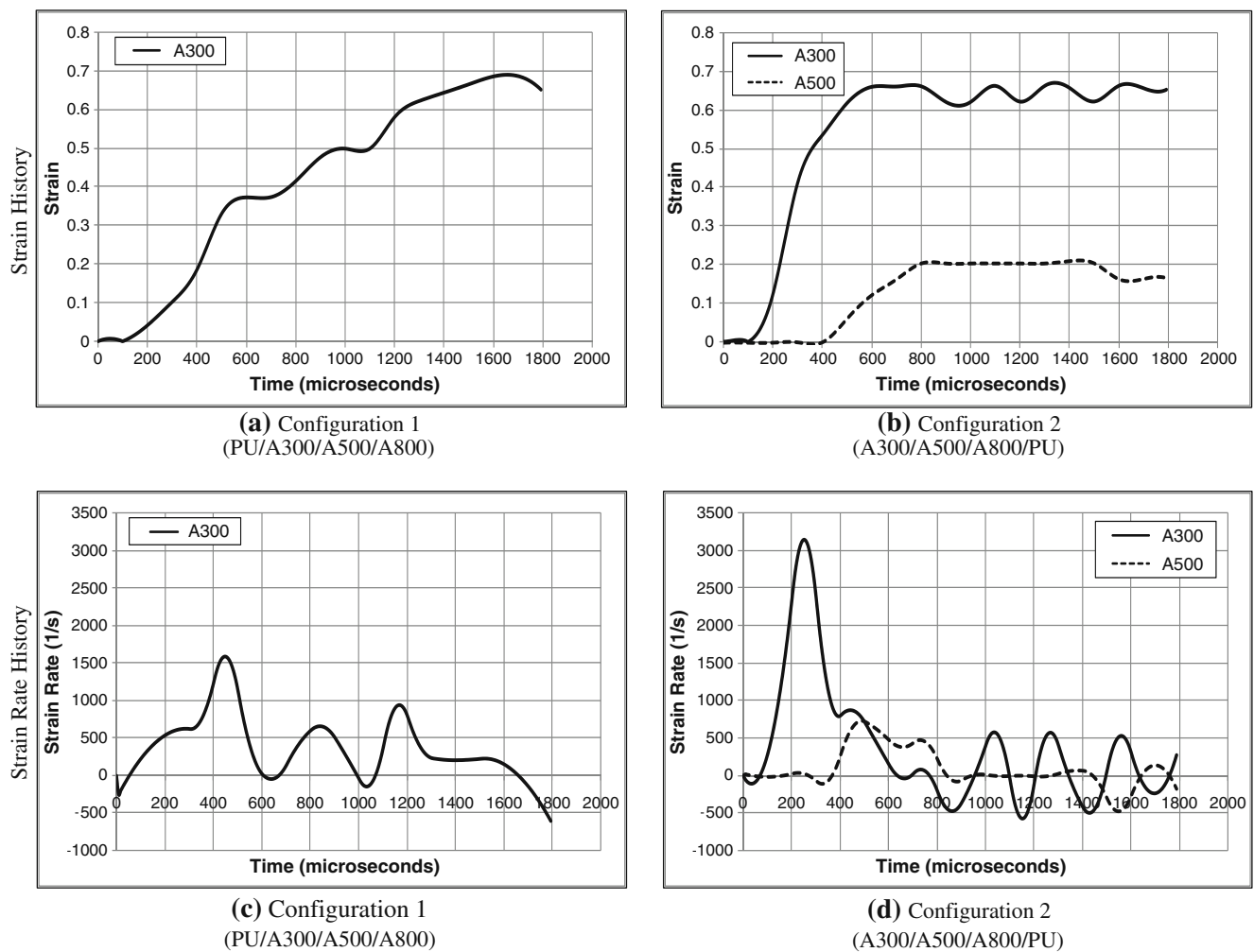


**Fig. 12** Strain and strain rate history of each core layer along the mid-line (line of symmetry) for both configurations

much higher strain rate than the A300 layer of configuration 1, which was expected since the maximum level of strain in configuration 2 was achieved approximately twice as fast ( $\sim 800 \mu\text{s}$  earlier) than in configuration 1. It should be noted that in configuration 2 the core stops compressing by approximately  $t=800 \mu\text{s}$ , thus the oscillations that are observed in the strain rate plot after this time can be correlated to the errors in data recording, and consequently neglected.

From the mid-point deflection data in Fig. 11(a) and (b), the average mid-point velocities of the front face and back face for both configurations can be obtained by differentiating the front face and back face deflection with respect to time, and are shown in Fig. 13. It can be seen in the figure that in configuration 1, the front face and back face reach a maximum velocity together early in the deformation history,  $\sim t=700 \mu\text{s}$ , converging on the same common velocity ( $\sim 30 \text{ m/s}$ ) and then decelerating together. The front face and back face of configuration 2 reach maximum velocities at different times,  $\sim t=400 \mu\text{s}$  and  $\sim t=600 \mu\text{s}$  respectively, and then share a common velocity of  $\sim 20 \text{ m/s}$  much later in the

event ( $\sim 800 \mu\text{s}$ ), before decelerating together. This suggests that the back face was beginning to decelerate, while the core was still compressing. Such responses and phenomena have been investigated by Liang et al. [20] and Tilbrook et al. [21]. When the front and back face velocities equalize early in the deformation history, this response is labeled as a hard core type response. In contrast, when the back face begins to decelerate while the core is still compressing, this response is labeled as a soft core type response. Therefore it can be concluded that configuration 1 exhibits a hard core type response, while configuration 2 exhibits a soft core type response. The authors [20, 21] suggested that the optimal performance of sandwich beams is attained for soft core designs, which allows for a reduction in the transmitted impulse during the initial fluid-structure interaction stage.

#### Digital Image Correlation (DIC) analysis

Utilizing the Digital Image Correlation (DIC) technique, the full-field deflection, in-plane strain and particle velocity

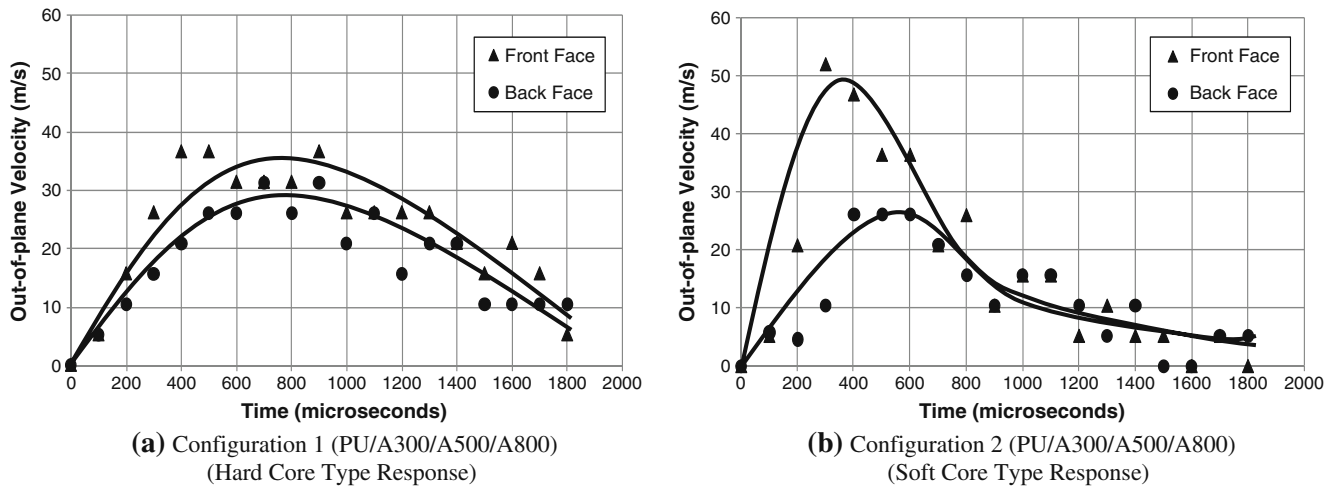


Fig. 13 Front and back face out-of-plane velocities for both configurations

contours of the back facesheet for each configuration were generated. Figures 14, 15 and 16 show the full-field results for the back facesheet of configuration 1 and configuration 2 respectively. Figure 14 shows the full-field out-of-plane deflection ( $W$ ) with a scale of 0 mm (purple) to 32 mm (red). It is evident from the figure that for configuration 1, as shown in Fig. 14(a), the back face exhibits very little out-

of-plane deflection until approximately  $t=400 \mu\text{s}$ . Between  $t=400 \mu\text{s}$  and  $t=1800 \mu\text{s}$ , the panel continues to show deflection. By  $t=1800 \mu\text{s}$ , it can be observed that the central region of the panel has deflected approximately 32 mm. For configuration 2, as shown in Fig. 14(b), the back face shows very little out-of-plane deflection until  $t=400 \mu\text{s}$ . Between  $t=400 \mu\text{s}$  and  $t=1800 \mu\text{s}$ , the panel

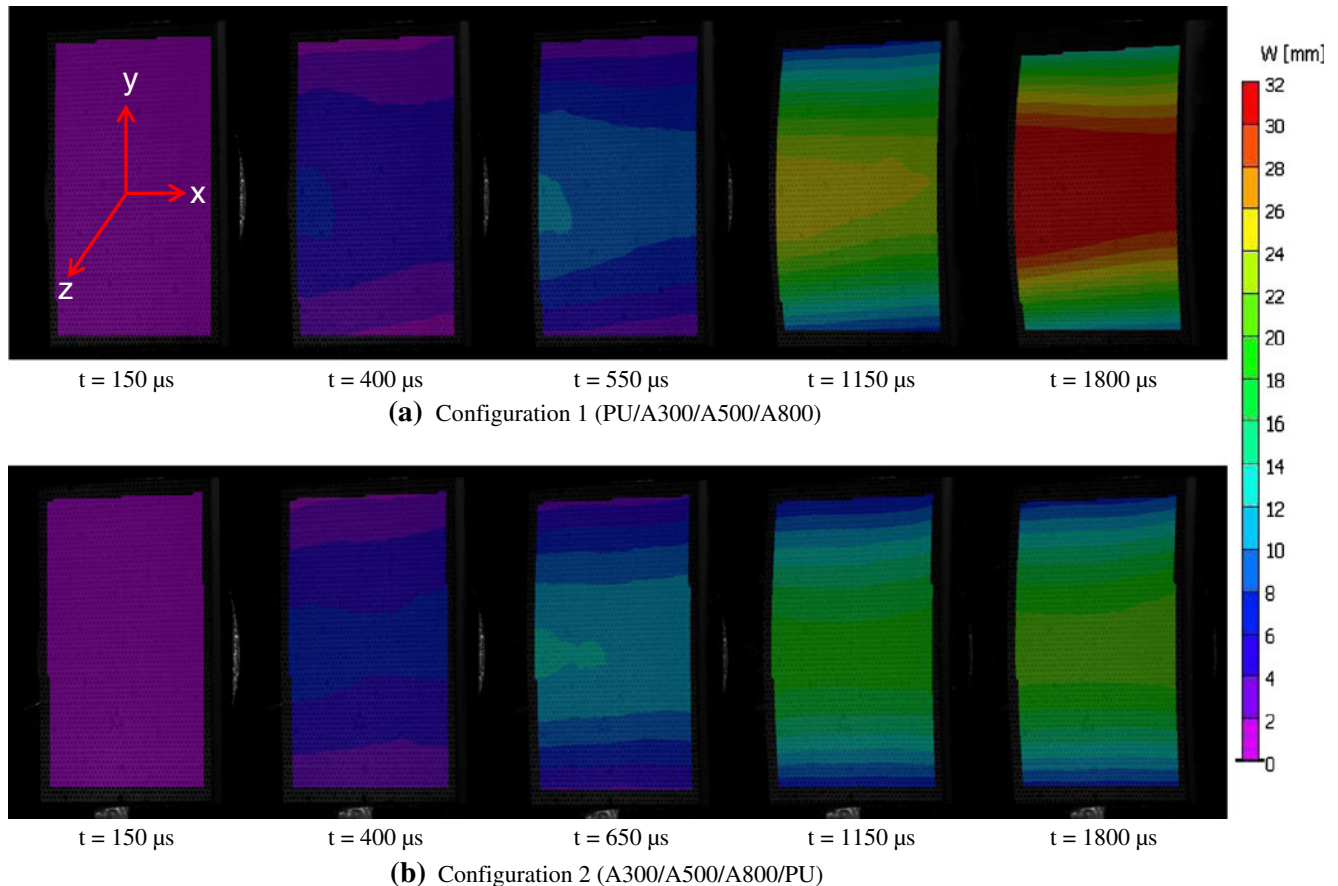
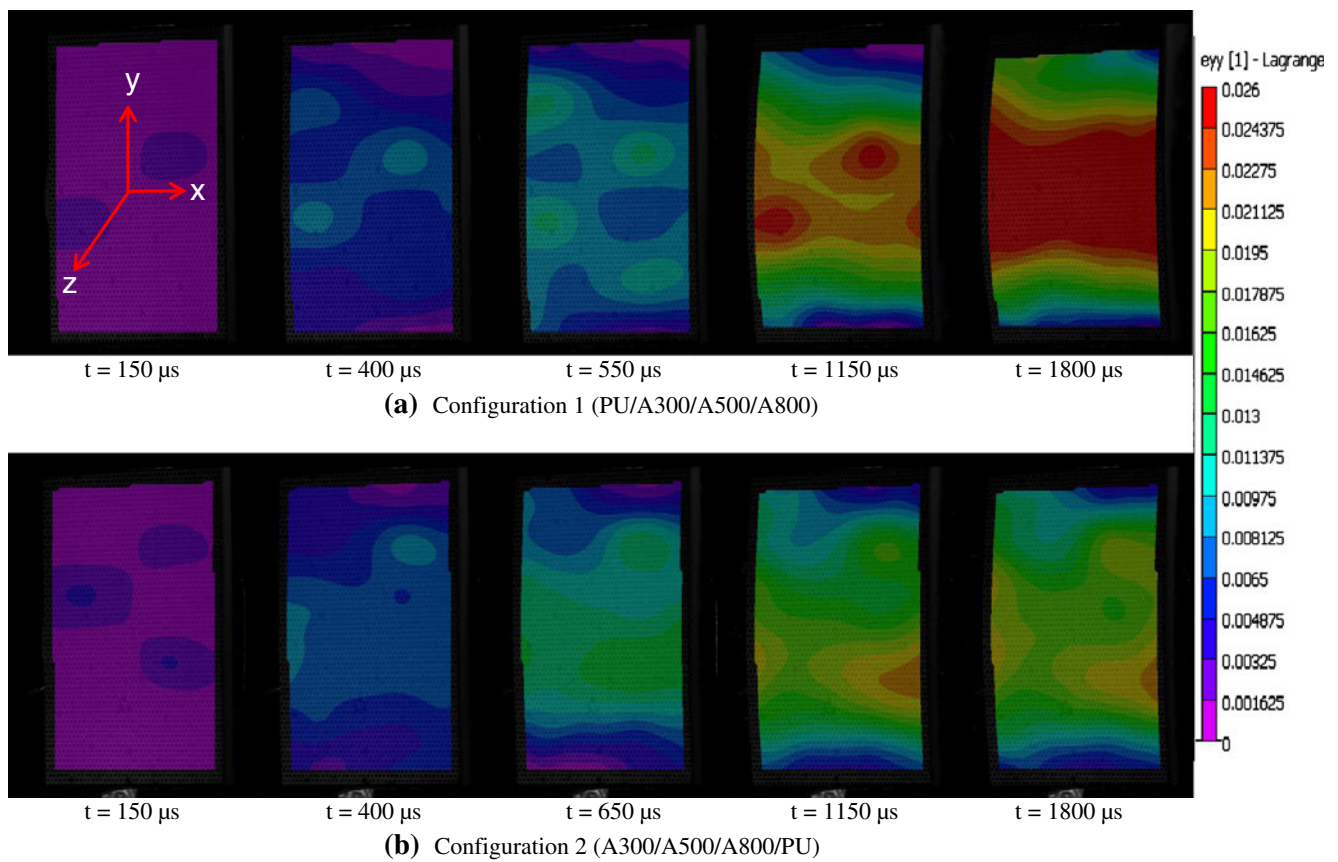


Fig. 14 Full-field out-of-plane deflection ( $W$ ) of both configurations



**Fig. 15** Full-field in-plane-strain ( $\epsilon_{yy}$ ) of both configurations

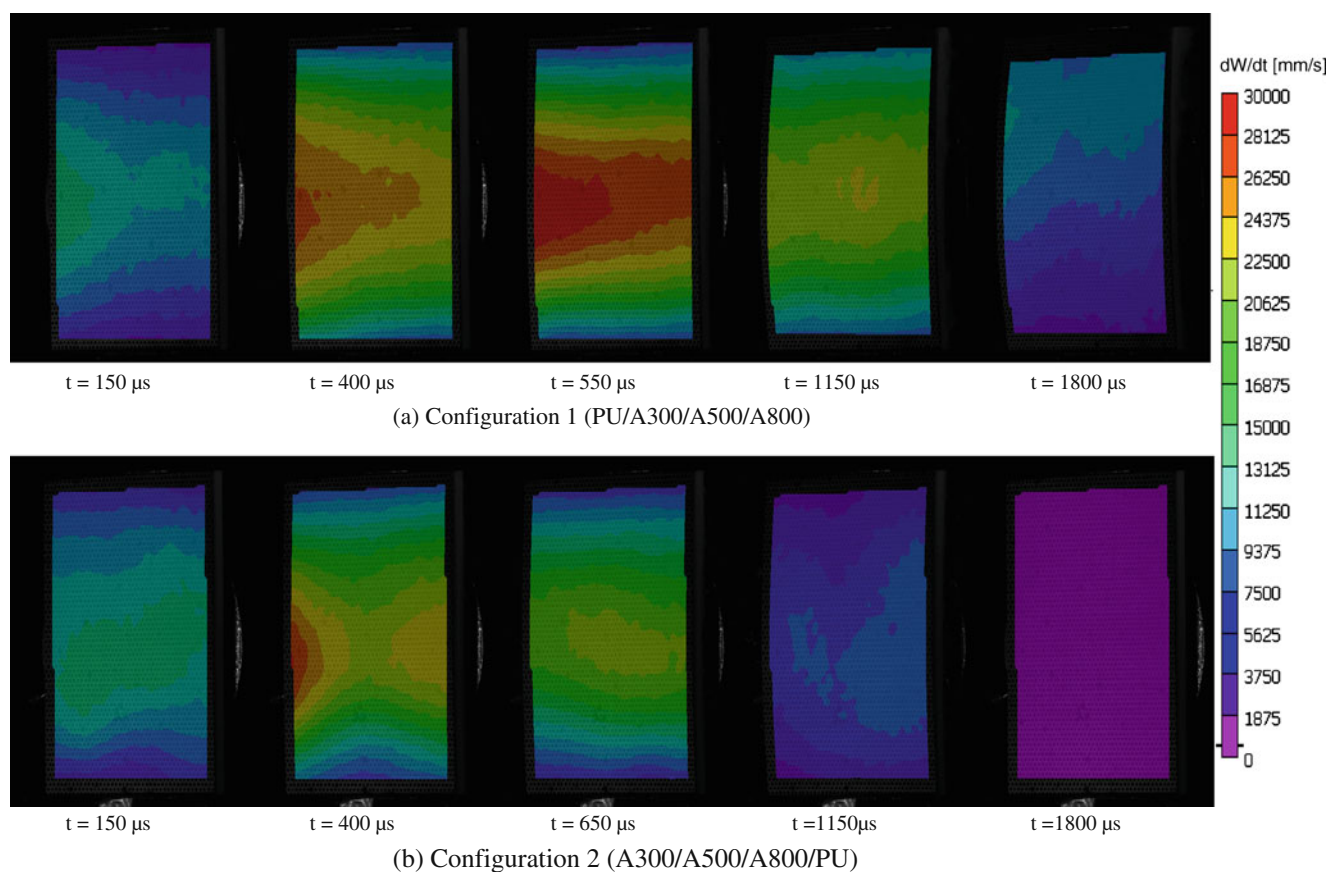
continues to exhibit deflection. By  $t=1800 \mu\text{s}$ , the central region of the panel has deflected approximately 22 mm. Therefore, configuration 2 deflects approximately 35% less than configuration 1.

Figure 15 shows the full-field in-plane-strain ( $\epsilon_{yy}$ ) for both configurations with a scale of 0 (red) to 0.026 (purple), or 0% to 2.6% respectively. For configuration 1, as shown in Fig. 15(a), the back face exhibits very minimal in-plane-strain ( $\epsilon_{yy}$ ) until approximately  $t=150 \mu\text{s}$ . Between  $t=150 \mu\text{s}$  and  $t=1800 \mu\text{s}$ , the in-plane-strain ( $\epsilon_{yy}$ ) continues to increase. By  $t=1800 \mu\text{s}$ , it can be observed that the panel shows a maximum in-plane-strain ( $\epsilon_{yy}$ ) across the central region of the panel of approximately 2.6%. For configuration 2, as shown in Fig. 15(b), the back face shows very minimal in-plane-strain ( $\epsilon_{yy}$ ) until approximately  $t=150 \mu\text{s}$ . Between  $t=150 \mu\text{s}$  and  $t=1800 \mu\text{s}$ , the in-plane-strain ( $\epsilon_{yy}$ ) continues to increase. By  $t=1800 \mu\text{s}$ , the panel shows a maximum in-plane-strain ( $\epsilon_{yy}$ ) across the central region of the panel of approximately 1.625%. As a result, configuration 2 exhibits approximately 35% in-plane-strain than configuration 1.

The full-field out-of-plane velocity ( $dW/dt$ ) of the back face is shown in Fig. 16 for both configurations with a scale from 0 mm/s (purple) to 30,000 mm/s (red), or 0 m/s to 30 m/s. For configuration 1, as shown in Fig. 16(a), the

back face begins to exhibit out-of-plane velocity by  $t=150 \mu\text{s}$ . By  $t=550 \mu\text{s}$ , the central region of the back face has reached an out-of-plane velocity of approximately 30 m/s. By  $t=1150 \mu\text{s}$  the velocity has reduced to approximately 22.5 m/s and by  $t=1800 \mu\text{s}$  the velocity has reduced to 7.5 m/s. For configuration 2, as shown in Fig. 16(b), the back face begins to show out-of-plane velocity by  $t=150 \mu\text{s}$ . By  $t=400 \mu\text{s}$ , the central region of the back face has reached an out-of-plane velocity of approximately 24.375 m/s. From  $t=400 \mu\text{s}$  and onward, the out-of-plane back face velocity continues to be reduced to approximately 22.5 m/s at  $t=650 \mu\text{s}$ , approximately 7.5 m/s at  $t=1150 \mu\text{s}$ , and approximately 0 m/s by  $t=1800 \mu\text{s}$ . Subsequently, configuration 2 reduces the back face velocity by approximately 15% in comparison to configuration 1.

Utilizing a point-inspection tool from digital image correlation, the data at the center point of the back facesheet for each configuration was evaluated and plotted. The out-of-plane deflection, as well as the back face velocity, showed excellent agreement with the results generated utilizing the side-view high speed images, and therefore only the in-plane strain results are shown in Fig. 17. The back face of configuration 1 exhibits a maximum in-plane strain ( $\epsilon_{yy}$ ) of approximately 2.4% at  $t=1800 \mu\text{s}$ . For



**Fig. 16** Full-field out-of-plane velocity ( $dW/dt$ ) of both configurations

configuration 2, the back face shows a maximum in-plane-strain ( $\epsilon_{yy}$ ) of approximately 1.6% at  $t=1800 \mu s$ . Configuration 2 exhibits approximately 35% less in-plane-strain ( $\epsilon_{yy}$ ) than configuration 1.

#### Post mortem analysis

After the blast loading event occurred, the damage patterns of both configuration 1 and configuration 2 were

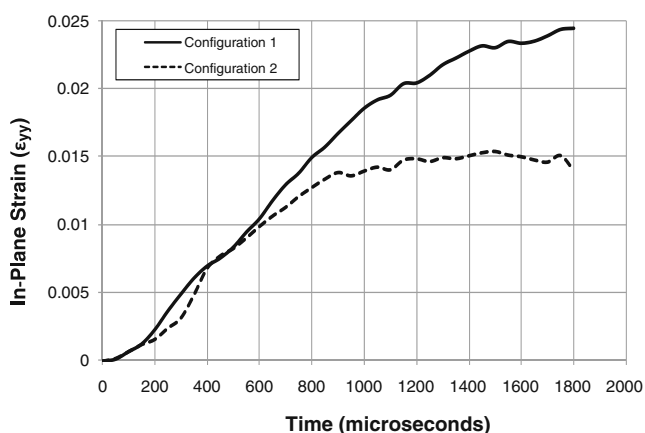


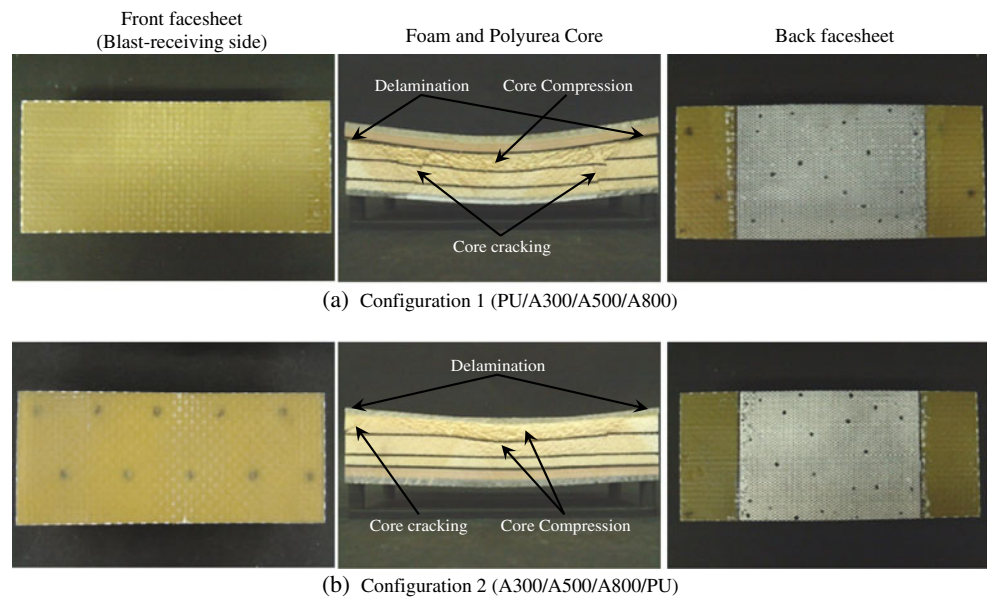
**Fig. 17** In-plane strain ( $\epsilon_{yy}$ ) of both configurations

visually examined and recorded using a high resolution digital camera and are shown in Fig. 18. When configuration 1 was subjected to transient shock wave loading, as shown in Fig. 18(a), the damage was confined to the areas where the supports were located in the shock tube apparatus and core cracking is visible in these two areas. The core cracks propagated completely through the foam core to the polyurea interlayer. Core delamination is visible between the polyurea interlayer, and the first layer of the foam core (A300). Core compression is visible in the first core layer of A300 foam.

When configuration 2 was subjected to transient shock wave loading, the damage patterns can be seen in Fig. 18 (b). For this configuration, very little core damage was observed. Core delamination between the first two layers of the foam core (A300 and A500) led to a crack that propagated through the first foam core layer (A300) to the front facesheet. Skin delamination was evident between the front face and the first foam core layer (A300). Also core compression can be observed in the first two layers of the foam core (A300 and A500).

Figure 19 shows the damage patterns of both configuration 1 and configuration 2 after they were subjected to the higher levels of blast loading (incident peak pressure  $\sim 1.5$  MPa, reflected peak pressure  $\sim 7.5$  MPa, wave velocity

**Fig. 18** Visual examination of both configurations after being subjected to high intensity blast load (Incident peak pressure  $\sim 1.0$  MPa)



of 1300 m/s). It can be seen from the figure that when configuration 1, as seen in Fig. 19(a), was subjected to a higher level of blast loading, the core exhibited heavy core cracking which lead to catastrophic failure. The front face showed heavy fiber delamination and cracking across the central region, while the back face delaminated completely from the core.

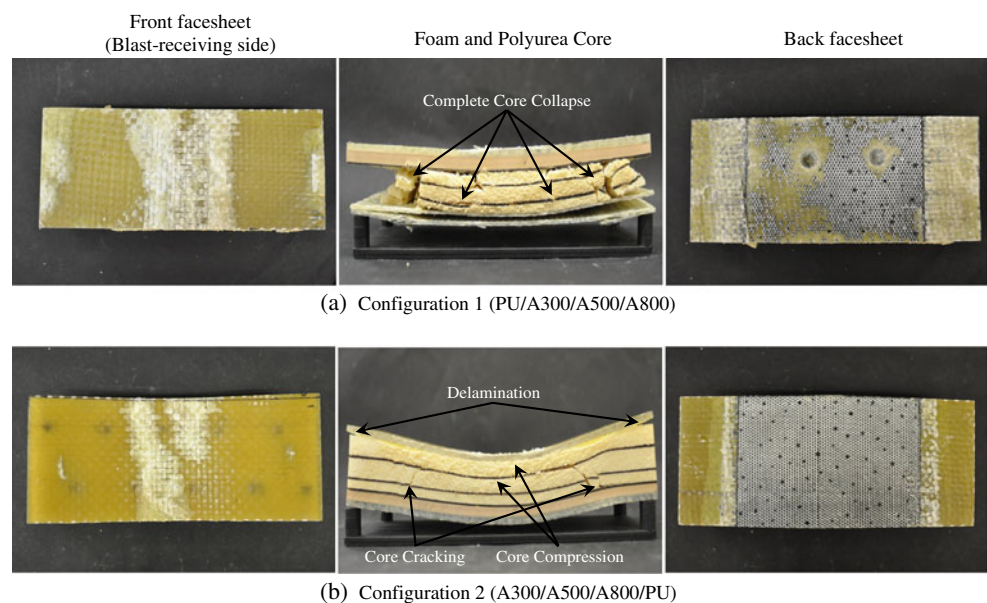
Configuration 2 on the other hand, as seen in Fig. 19(b), remained structurally intact after the higher level of blast loading. The front face showed minor fiber delamination, while the core exhibited cracking along the central region where the supports were located. Minor front skin delamination was evident between the front face and the first foam core layer (A300). Also core compression can be

observed in the first and second core layers of foam, A300 and A500 respectively.

#### *Energy redistribution behavior*

The energy redistribution behavior of both configurations was next analyzed using the methods described by Wang et al. [22]. The total energy loss and the total deformation energy of both configuration 1 and configuration 2 during the blast loading event are shown in Figs. 20 and 21 respectively. Total energy loss is characterized as the difference between the incident and remaining energies of the gas and total deformation energy is defined as the work done by the gas to deform the specimen. It can be observed

**Fig. 19** Visual examination of both configurations after being subjected to high intensity blast load (Incident peak pressure  $\sim 1.5$  MPa)



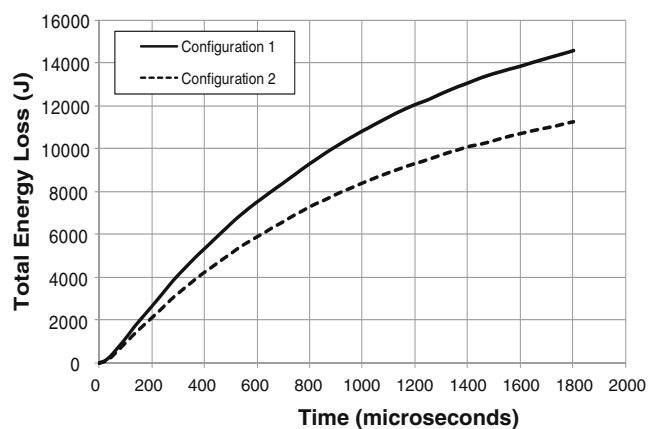


**Fig. 20** Total energy loss in both configurations during blast loading event

in Figs. 20 and 21 that at  $t=1800 \mu\text{s}$ , the total energy loss of configuration 1, as well as the deformation energy, is approximately 25% more than that of configuration 2. This indicates that configuration 1 has the ability to consume more energy during the shock loading process, as discussed in “Real time deformation”, but results in heavier core damage as observed in Figs. 18(a) and 19(a). This phenomenon is directly related to the location of the polyurea layer and has been described by Amini et al. [13–16]. Polyurea is a highly pressure sensitive elastomer with its shear and bulk stiffness increasing remarkably with increasing pressure [8]. When polyurea is applied to the front of the specimen, behind the facesheet and in front of the foam core, the confined polyurea is loaded in compression, increasing its bulk stiffness and thus attaining a better impedance match with the facesheet. Consequently, more of the blast energy is transferred to the foam core.

On the contrary, when polyurea is applied to the back of the specimen, behind the foam core and in front of the facesheet, the foam core is loaded first and then a part of this energy is transferred to the polyurea. This compresses

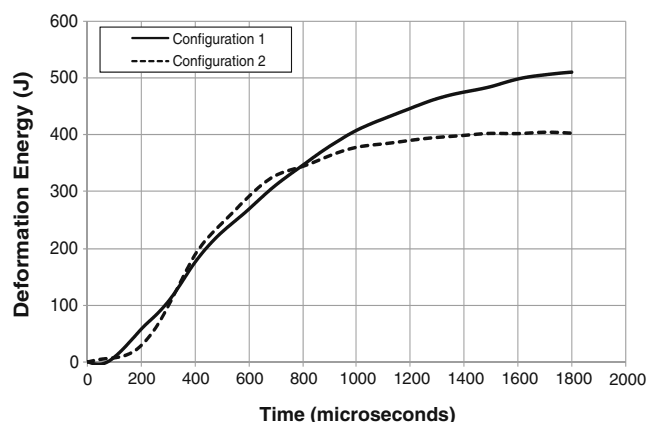


**Fig. 21** Deformation energy of both configurations during blast loading event

the polyurea layer, thus increasing its stiffness, and therefore increasing the amount of energy that it captures. This behavior can be elucidated by the fact that as the pressure-pulse travels through the polyurea layer and subsequently through the back facesheet, it is reflected back off its free-face as a tensile release wave. This results in a substantial decrease in the polyurea’s shear stiffness and concurrently substantial increase in its dissipative ability due to its viscoelasticity. This phenomenon can be observed in the overall behavior of configuration 2. From the high speed images in Fig. 10, it can be seen that the foam core is loaded first, resulting in heavy core compression as discussed in “Real time deformation” and shown in Figs. 18(b) and 19(b). In comparison to configuration 1, the peak values of back face deflection, strain and velocity are reduced by 35%, 35% and 15% respectively, as shown in Figs. 11(b), 13(b) and 17. This means the energy that is transferred to the back face of configuration 2 is less than that of configuration 1.

Therefore, it can be concluded that the location of the polyurea layer has a significant positive effect on the response of composite sandwich panels to shock wave loading, both in terms of failure mitigation and energy absorption, if it is placed opposite the blast-receiving side (configuration 2). On the contrary, the presence of polyurea on the blast-receiving side (configuration 1), amplifies the destructive effect of the blast, promoting (rather than mitigating) the failure of the composite sandwich panels.

## Conclusions

The following is the summary of the investigation:

- (1) The dynamic stress-strain response is significantly higher than the quasi-static response for each type of core material used in the present study, Corecell™ A-series foam and Dragonshield-HT polyurea respectively. The quasi-static and dynamic constitutive behaviors of Corecell™ A-series foams (A300, A500, and A800) as well as the polyurea interlayer show an increasing trend. The increase in the yield strength from quasi-static response to dynamic response, along with the longer stress plateau, indicates that these core materials show great potential in absorbing large amounts of energy.
- (2) Sandwich composites with two types of core layer arrangements were subjected to shock wave loading. Both core configurations consisted of three (3) types of Corecell™ foam and a polyurea (Dragonshield—HT) interlayer. The foam core was monotonically graded based on increasing wave impedance, and the only difference between the two core configurations

arose in the location of the polyurea interlayer. It was observed that when the polyurea interlayer is located behind the graded foam core, and in front of the back face (i.e. configuration 2), the core layer arrangement allows for a stepwise compression of the core. Larger compression was visible in the A300 and A500 foam core layers of configuration 2 than configuration 1. This compression lowers the strength of the initial shock wave by the time it reaches the back facesheet and thus the overall deflection, in-plane strain, and velocity were reduced in comparison to the sandwich composite with the polyurea interlayer located behind the front facesheet and in front of the foam core (i.e. configuration 1). Therefore it can be concluded that placing the polyurea interlayer behind the foam core and in front of the back facesheet (configuration 2) improves the blast resistance of the sandwich composite and better maintains structural integrity.

- (3) Comparison of the mid-point deflection of both configurations was made using high-speed photography (side-view images) and the Digital Image Correlation (DIC) technique. Results obtained using both methods of analysis showed excellent agreement with a small margin of error (<5%).
- (4) The methods used to evaluate the energy as described by Wang et al. [22] were implemented and the results analyzed. It was observed that the location of the polyurea layer has a significant positive effect on the response of composite sandwich panels to shock wave loading, both in terms of failure mitigation and energy absorption, if it is placed opposite the blast-receiving side (configuration 2). On the contrary, the presence of polyurea on the blast-receiving side (configuration 1), amplifies the destructive effect of the blast, promoting (rather than mitigating) the failure of the composite sandwich panels.

**Acknowledgement** The authors kindly acknowledge the financial support provided by Dr. Yapa D. S. Rajapakse, under Office of Naval Research Grant No. N00014-04-1-0268. The authors acknowledge the support provided by the Department of Homeland Security under Cooperative Agreement No. 2008-ST-061-ED0002. Authors thank Gurit SP Technology and Specialty Products Incorporated (SPI) for providing the material as well as Dr. Stephen Nolet and TPI Composites for providing the facility for creating the composites used in this study.

## References

1. Xue Z, Hutchinson JW (2003) Preliminary assessment of sandwich plates subject to blast loads. *Int J Mech Sci* 45:687–705
2. Fleck NA, Deshpande VS (2004) The resistance of clamped sandwich beams to shock loading. *J Appl Mech* 71:386–401
3. Dharmasena KP, Wadley HNG, Xue Z, Hutchinson JW (2008) Mechanical response of metallic honeycomb sandwich panel structures to high-intensity dynamic loading. *Int J Imp Eng* 35 (9):1063–1074
4. Apetre NA, Sankar BV, Ambur DR (2006) Low-velocity impact response of sandwich beams with functionally graded core. *Int J Solid Struct* 43(9):2479–2496
5. Li Y, Ramesh KT, Chin ESC (2001) Dynamic characterization of layered and graded structures under impulsive loading. *Int J Solid Struct* 38(34–35):6045–6061
6. Wang E, Gardner N, Shukla A (2009) The blast resistance of sandwich composites with stepwise graded cores. *Int J Solid Struct* 46:3492–3502
7. Yi J, Boyce MC, Lee GF, Balizer E (2005) Large deformation rate-dependent stress-strain behavior of polyurea and polyurethanes. *Poly* 47(1):319–329
8. Amirkhizi AV, Isaacs J, McGee J, Nemat-Nasser S (2006) An experimentally-based constitutive model for polyurea, including pressure and temperature effects. *Phil Mag* 86(36):5847–5866
9. Hoo Fatt MS, Ouyang X, Dinan RJ (2004) Blast response of walls retrofitted with elastomer coatings. *Struct Mater* 15:129–138
10. Roland CM, Twigg JN, Vu Y, Mott PH (2006) High strain rate mechanical behavior of polyurea. *Poly* 48(2):574–578
11. Tekalur SA, Shukla A, Shivakumar K (2008) Blast resistance of polyurea based layered composite materials. *Comp Struct* 84:271–281
12. Bahei-El-Din YA, Dvorak GJ, Fredricksen OJ (2006) A blast-tolerant sandwich plate design with a polyurea interlayer. *Int J Solid Struct* 43:7644–7658
13. Amini MR, Isaacs JB, Nemat-Nasser S (2010) Experimental investigation of response of monolithic and bilayer plates to impulsive loading. *Int J Imp Eng* 37:82–89
14. Amini MR, Amirkhizi AV, Nemat-Nasser S (2010) Numerical modeling of response of monolithic and bilayer plates to impulsive loading. *Int J Imp Eng* 37:90–102
15. Amini MR, Isaacs JB, Nemat-Nasser S (2010) Numerical modeling of effect of polyurea on response of steel plates to impulsive loads in direct pressure-pulse experiments. *Mech Mater* 42:615–627
16. Amini MR, Isaacs JB, Nemat-Nasser S (2010) Investigation of effect of polyurea on response of steel plates to impulsive loads in direct pressure-pulse experiments. *Mech Mater* 42:628–639
17. <http://www.gurit.com/page.asp?section=00010001002200160009&sectionTitle=Corecell%99+A-Foam+--+For+Hulls+%26+Dynamic+Loading>. Accessed 21 Dec 2010.
18. <http://www.specialty-products.com/polyurea-products/Polyurea-Plural-Component-Coatings/dragonshield-ht-erc/>. Accessed 21 Dec 2010.
19. Chen W, Zhang B, Forrestal MJ (1999) A split hopkinson bar technique for low impedance materials. *Exp Mech* 39(2):81–85
20. Liang Y, Spuskanyuk AV, Flores SE, Hayhurst DR, Hutchinson JW, McMeeking RM, Evans AG (2007) The response of metallic sandwich panels to water blast. *J Appl Mech* 74:81–99
21. Tilbrook MT, Deshpande VS, Fleck NA (2006) The impulsive response of sandwich beams: analytical and numerical investigation of regimes of behavior. *J Mech Phys Sol* 54:2242–2280
22. Wang E, Shukla A (2010) Analytical and experimental evaluation of energies during shock wave loading. *Int J Imp Eng* 37:1188–1196